To appear in *Molecular Physics*
Vol. 00, No. 00, Month 2015, 1–12

RESEARCH ARTICLE

Electron Localisation Function in Current-Density-Functional Theory

James W. Furness[a] Ulf Ekström[b], Trygve Helgaker[b] and Andrew M. Teale[ab]*

[a]*School of Chemistry, University of Nottingham, University Park, Nottingham, NG7 2RD, UK*;
[b]*Centre for Theoretical and Computational Chemistry, Department of Chemistry, University of Oslo, P. O. Box 1033, Blindern, N-0315, Oslo, Norway*
(*Received 00 Month 200x; final version received 00 Month 200x*)

We present a generalisation of the electron localisation function (ELF) to current-density-functional theory as a descriptor for the properties of molecules in the presence of magnetic fields. The resulting current ELF (cELF) is examined for a range of small molecular systems in field strengths up to $B_0 = 235\,\mathrm{kT}$ (one atomic unit). The cELF clearly depicts the compression of the molecular electronic structure in the directions perpendicular to the applied field and exhibits a structure similar to that of the physical current densities. A topological analysis is performed to examine the changes in chemical bonding upon application of a magnetic field.

Keywords: chemical bonding, electron localisation function, density-functional theory, current density-functional theory, molecular magnetic properties

1. Introduction

The electron localisation function (ELF), introduced for Hartree–Fock theory by Becke and Edgecombe [1] and extended to Kohn–Sham density-functional theory (DFT) via an alternative interpretation due to Savin [2], has enjoyed enormous success as a tool for understanding and visualising chemical bonding. The ELF has been widely applied to understand bonding in atoms [3], molecules [4–9], clusters [10–13], and solid-state structures [14, 15]. A topological analysis of ELF in the spirit of Bader's atoms-in-molecules approach [16] yields further information on bonding in a given system [2, 17–20], although some caution should be exercised in interpretations based on this analysis [21].

Recently, we have studied exchange–correlation functionals in current DFT (CDFT) for calculations of molecules in the presence of strong uniform magnetic fields [22–25]. In particular, in Ref. [25], we showed that the current-dependent generalisation of the Tao–Perdew–Staroverov–Scuseria (TPSS) meta-generalised-gradient-approximation (meta-GGA) functional [26], denoted cTPSS (see also Ref. [27] for the use of cTPSS in response theory) provides a reasonable description of molecules in strong magnetic fields. In such fields, a new form of bonding, perpendicular paramagnetic bonding, has recently been identified [28]. The nature of this bonding interaction was accurately captured and analysed in terms of

*Corresponding author. Email: andrew.teale@nottingham.ac.uk

ISSN: 00268976 print/ISSN 13623028 online

DOI: 10.1080/0026897YYxxxxxxxx
http://www.informaworld.com

molecular-orbital energies and electron-density differences at the CDFT level in Ref. [25] using the cTPSS functional.

In Section 2, we propose a generalisation of the ELF for molecules in a magnetic field. This generalisation is applied to study chemical bonding in Section 3.1, whereas a topological analysis is performed in Section 3.2. Finally, in Section 3.3, the physical current density induced by the field is visualised alongside the generalised ELF, illustrating the striking similarity in the topologies of these quantities.

2. Theory

After reviewing the ELF as introduced in Hartree–Fock theory in Sec. 2.1, we consider its adaption for Kohn–Sham theory in Sec. 2.2. Finally, we discuss the generalisation of the ELF to systems in magnetic fields in Sec. 2.3.

2.1. *ELF in Hartree–Fock theory*

The definition of the ELF by Becke and Edgecombe [1] focused on Hartree–Fock theory and the same-spin pair density,

$$P_2^{\sigma\sigma}(\mathbf{r},\mathbf{r}') = \rho_\sigma(\mathbf{r})\rho_\sigma(\mathbf{r}') - |\rho_1^\sigma(\mathbf{r},\mathbf{r}')|^2, \quad \rho_1^\sigma(\mathbf{r},\mathbf{r}') = \sum_{i=1}^{N_\sigma} \varphi_{i\sigma}^*(\mathbf{r}')\varphi_{i\sigma}(\mathbf{r}). \tag{1}$$

Expansion of the spherically averaged same-spin conditional pair density

$$P_{\mathrm{cond}}^{\sigma\sigma}(\mathbf{r},\mathbf{r}') = \rho_\sigma(\mathbf{r}') - \frac{|\rho_1^\sigma(\mathbf{r},\mathbf{r}')|^2}{\rho_\sigma(\mathbf{r})} \tag{2}$$

to leading order gives

$$P_{\mathrm{cond}}^{\sigma\sigma}(\mathbf{r},s) = \frac{1}{3}\left[\sum_{i=1}^{N_\sigma} |\nabla\varphi_{i\sigma}(\mathbf{r})|^2 - \frac{1}{4}\frac{|\nabla\rho_\sigma(\mathbf{r})|^2}{\rho_\sigma(\mathbf{r})}\right] s^2 + \cdots = \frac{1}{3}D_\sigma(\mathbf{r})s^2\ldots, \tag{3}$$

where s is the radius of a spherical shell around $\mathbf{r}$. The term in brackets is related to the Fermi-hole curvature derived by Becke [29] and generalised by to non-zero current densities by Dobson [30]. Becke and Edgecombe [1] proposed to use this term as a measure of electron localisation, introducing the relative ELF measure

$$f_{\mathrm{ELF},\sigma}(\mathbf{r}) = \frac{1}{1+[D_\sigma(\mathbf{r})/D_\sigma^0(\mathbf{r})]^2}. \tag{4}$$

Here $D_\sigma(\mathbf{r})$ is defined in Eq. (3), while $D_\sigma^0(\mathbf{r})$ is the corresponding quantity for a homogeneous electron gas

$$D_\sigma^0(\mathbf{r}) = 2^{5/3}c_{\mathrm{F}}\rho_\sigma(\mathbf{r})^{5/3}, \quad c_{\mathrm{F}} = \frac{3}{10}(3\pi^2)^{2/3}. \tag{5}$$

Defined in this manner, the ELF is a dimensionless quantity between 0 and 1. The upper limit $f_{\mathrm{ELF},\sigma}(\mathbf{r}) = 1$ corresponds to perfect localisation, whereas $f_{\mathrm{ELF},\sigma}(\mathbf{r}) = 0.5$ indicates behaviour close to that of a uniform gas with the same density.

2.2. *ELF in Kohn–Sham theory*

The ELF as proposed for Hartree–Fock theory relies on the definition of the conditional pair-density, $P^{\sigma\sigma}_{\mathrm{cond}}(\mathbf{r}, s)$, for the interacting system. This quantity is not accessible in the same manner in Kohn–Sham DFT, since the determinantal wave function is then used to describe a system of *non-interacting* electrons rather than to approximate the physical system. On the other hand, Savin *et al.* [14] noted that the leading term in Eq. (3) is accessible in Kohn–Sham theory, being related in a simple manner to the Pauli kinetic-energy density:

$$\tau_\sigma^{\mathrm{Pauli}}(\mathbf{r}) = \tau_\sigma(\mathbf{r}) - \tau_\sigma^{\mathrm{vW}}(\mathbf{r}) = \frac{1}{2} D_\sigma(\mathbf{r}) \tag{6}$$

where

$$\tau_\sigma(\mathbf{r}) = \frac{1}{2}\sum_{i=1}^{N_\sigma} |\nabla\varphi_{i\sigma}(\mathbf{r})|^2, \quad \tau_\sigma^{\mathrm{vW}}(\mathbf{r}) = \frac{1}{8}\frac{|\nabla\rho_\sigma(\mathbf{r})|^2}{\rho_\sigma(\mathbf{r})}, \tag{7}$$

The term $\tau_\sigma(\mathbf{r})$ is the σ-spin contribution to the non-interacting kinetic-energy density in the everywhere-positive gauge. Integration of this quantity over all space yields the σ-spin component of the non-interacting kinetic energy T_s used in Kohn–Sham theory. This form reflects the fact that, although non-interacting, the Kohn–Sham wave function is a single Slater determinant, preserving the fermionic characteristics of the electrons. The second term in Eq. (6), $\tau_\sigma^{\mathrm{vW}}(\mathbf{r})$, is the von Weizsäcker (vW) kinetic-energy density, which can be interpreted as the kinetic-energy density for a system of bosonic particles with orbitals proportional to $\sqrt{\rho_\sigma}$. The difference in Eq. (6) can then be interpreted as the *change in the kinetic-energy density induced by the Pauli principle*. Since the von Weizsäcker kinetic-energy density provides a lower bound on the non-interacting kinetic energy density,

$$\tau_\sigma(\mathbf{r}) \geq \tau_\sigma^{\mathrm{vW}}(\mathbf{r}), \tag{8}$$

the Pauli kinetic-energy density is everywhere nonnegative.

Given that $\tau_\sigma^{\mathrm{Pauli}}(\mathbf{r})$ contains the same information as does $D_\sigma(\mathbf{r})$, we may consider whether the ratio $D_\sigma(\mathbf{r})/D^0_\sigma(\mathbf{r})$ required for $f_{\mathrm{ELF},\sigma}(\mathbf{r})$ may be derived from it. Savin *et al.* [14] noted that this can indeed be achieved by using the kinetic-energy density of a uniform electron gas

$$\tau_\sigma^{\mathrm{UEG}}(\mathbf{r}) = 2^{2/3} c_\mathrm{F} \rho_\sigma^{5/3} = \frac{1}{2} D^0_\sigma(\mathbf{r}), \tag{9}$$

yielding

$$\frac{D_\sigma(\mathbf{r})}{D^0_\sigma(\mathbf{r})} = \frac{\tau_\sigma^{\mathrm{Pauli}}(\mathbf{r})}{\tau_\sigma^{\mathrm{UEG}}(\mathbf{r})}. \tag{10}$$

The ELF may then be interpreted as a measure of localisation that reflects changes arising from the fermionic nature of the electrons and the satisfaction of the Pauli principle. This observation goes a long way towards rationalising the practical utility of $f_{\mathrm{ELF},\sigma}(\mathbf{r})$ for chemical interpretation, bearing in mind that the Pauli principle and its consequences govern many aspects of how chemical phenomena may be interpreted. The Pauli principle leads to Fermi-correlation (exchange) effects between electrons of the same-spin, which are typically an order of magnitude larger than

those between opposite-spin electrons (dynamical correlation). As a result, the interpretation of same-spin interactions, as in ELF, can serve as a useful qualitative tool for interpretation.

The ELF formula discussed above involves two separate functions, one for each spin. Kohout and Savin [3] proposed instead the spin-polarised form

$$f_{\mathrm{ELF}}(\mathbf{r}) = \frac{1}{1 + \left(\frac{\tau_\alpha^{\mathrm{Pauli}}(\mathbf{r}) + \tau_\beta^{\mathrm{Pauli}}(\mathbf{r})}{\tau_\alpha^{\mathrm{UEG}}(\mathbf{r}) + \tau_\beta^{\mathrm{UEG}}(\mathbf{r})} \right)^2}. \tag{11}$$

We consider closed-shell systems, for which the values of $f_{\mathrm{ELF}}(\mathbf{r})$ from Eqs. (4) and (11) are identical.

2.3. *Extension of ELF to magnetic fields*

In a magnetic field, $f_{\mathrm{ELF}}(\mathbf{r})$ becomes gauge dependent through its dependence on the kinetic energy density τ, itself a gauge variant quantity (see Refs. [25, 27, 30–34] for further discussion). This unphysical dependence can be removed by introducing terms dependent on the paramagnetic current density, such as those that arise in the discussion of the spherical average of the exchange hole by Dobson [30]. This can be accomplished either in the expansion of Eq. (3) or by replacing the first term of Eq. (6) according to

$$\tau_\sigma \rightarrow \tilde{\tau}_\sigma = \tau_\sigma - \frac{|\mathbf{j}_{\mathrm{p}\sigma}(\mathbf{r})|^2}{\rho_\sigma(\mathbf{r})} \tag{12}$$

where $\mathbf{j}_{\mathrm{p}\sigma}(\mathbf{r})$ is the paramagnetic current density,

$$\mathbf{j}_{\mathrm{p}\sigma}(\mathbf{r}) = -\frac{i}{2} \sum_i^{\mathrm{occ}} \left[\varphi_{i\sigma}^* \nabla \varphi_{i\sigma} - \varphi_{i\sigma} \nabla \varphi_{i\sigma}^* \right]. \tag{13}$$

This generalisation has previously been used to compute time-dependent ELFs [35, 36] and in the generalisation of meta-GGA functionals to calculate response properties perturbatively [27] and magnetic properties non-perturbatively [25]. The latter implementation allows for the self-consistent determination of molecular energies and orbitals in a magnetic field using London atomic orbitals [37–39] (also known as gauge-including atomic orbitals (GIAOs)). We note that the gauge independent kinetic energy density is not unique, and several other forms have been proposed [32, 34]. However, the choice Eq. (12) has the advantage that the kinetic energy density is independent of the external magnetic field, as well as satisfying Eq. (8). These issues have previously been examined in the context of meta-GGA functionals in Ref. [34]. Here, we use the cTPSS functional to perform calculations at a finite magnetic field, computing the generalised ELF as a function of field strength. Following the notation cTPSS for the TPSS functional with the substitution in (12), we use the acronym cELF for the similarly modified ELF.

3. Results

All cELF calculations use the LONDON program [40, 41] with the CDFT implementation of cTPSS described in Ref. [25] via the XCFun library [42] to determine the required quantities for ELF at different field strengths. All calculations have

been carried out in an uncontracted Cartesian aug-cc-pCVTZ basis set [43, 44] of London atomic orbitals [37]. Unless otherwise noted, zero-field TPSS geometries are used.

3.1. *Electron Confinement*

For a magnetic field of strength B along the z-axis, the molecular electronic Hamiltonian takes the form (in atomic units)

$$H = H_0 + \frac{1}{2}BL_z + BS_z + \frac{1}{8}B^2\sum_i(x_i^2 + y_i^2), \tag{14}$$

where H_0 is the unperturbed electronic Hamiltonian, $\frac{1}{2}BL_z$ is the orbital Zeeman operator expressed in terms of the orbital angular momentum operator L_z in the field direction, BS_z is the spin Zeeman operator expressed in terms of the spin angular momentum operator S_z in the field direction, and $\frac{1}{8}B^2\sum_i(x_i^2 + y_i^2)$ is the diamagnetic operator.

Whereas the Zeeman terms may raise or lower the energy, the diamagnetic term always raises the energy, becoming dominant in a field stronger than one atomic unit $B_0 \approx 235\,\mathrm{kT}$. From the form of the diamagnetic term, we see that the field confines the system in the directions perpendicular to the field vector. As a result, the field exerts a significant influence over the electronic structure and, in particular, the localisation of the electrons.

3.1.1. Paramagnetic Bonding

We first consider the recently discovered phenomenon of perpendicular paramagnetic bonding [28]. In Figure 1, we present iso-volumes for He_2 in a zero field (blue) and in a uniform field of strength B_0 perpendicular to the internuclear axis (red). The bond distance of $2.864a_0$ has been optimised at the cTPSS/u-aug-cc-pCVTZ level in the same field. In Ref. [28], the paramagnetic bonding in He_2 was rationalised in terms of induced electron rotation. The bonding was further analysed at the Kohn–Sham level in Ref. [25], in terms of molecular-orbital energies and density distortions relative to non-bonded atoms in the same field.

The confinement induced by the field, shown in red in Fig 1, is clearly captured by the cELF. In the field, the iso-surfaces contract around the atoms, becoming much more compact in the perpendicular directions than in the zero field (blue). Relaxation to the equilibrium geometry at zero field (not presented) gives similarly diffuse but near-spherical zero-field ELF iso-surfaces.

3.1.2. Covalent Bonding

To illustrate the utility of the cELF in understanding features of covalent bonding in magnetic fields, we consider methane, ethane, ethene, and ethyne as prototypical systems containing single, double, and triple bonds. In Figure 2, the methane results are shown. In the absence of a field, the blue iso-surfaces are consistent with those obtained in earlier studies; in the presence of field, the iso-surfaces around the atoms contract. The structure of the cELF is similar for ethane, see Figure 3. An additional region of electron localisation is seen at the centre of the C-C bond both at zero field and at $B = 0.4B_0$. As the field increases, the localisation becomes less pronounced, eventually splitting into two separate regions.

The zero-field ELF plots for ethene in Figure 4 are consistent with those presented elsewhere [2], with a characteristic dumb-bell shaped structure at the centre of the C=C bond. With increasing field strength, the dumb-bell structure splits into two,

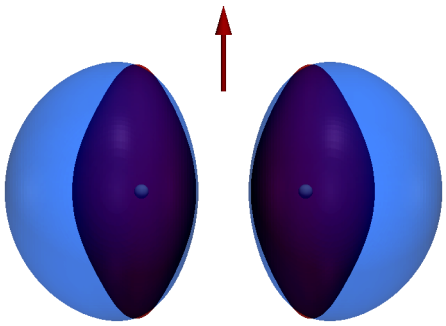

Figure 1. Perpendicular paramagnetic bonding in He_2. The iso-volumes depict the regions of $f_{\mathrm{ELF}} \geq 0.8$ at zero field (blue-lighter) and in the presence of a perpendicular magnetic field of strength B_0 (red-darker). The system is considered at the equilibrium geometry of $R = 2.864a_0$ as determined in a perpendicular field of $B = B_0$

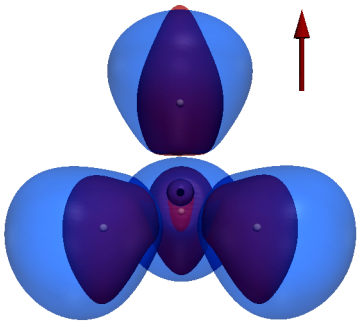

Figure 2. The cELF for methane calculated at the cTPSS/u-aug-cc-pCVTZ level at the corresponding zero-field geometry. The blue iso-volumes depict the regions of $f_{\mathrm{ELF}} \geq 0.8$ in the absence of a magnetic field (blue-lighter) and in a field of strength B_0 (red-darker). The direction of the field is indicated by the red arrow.

developing eventually into two new structures with localisation above and below the C=C bond. Around the hydrogen atoms, the cELF surfaces of ethene contract in a manner similar to that observed for methane and ethane.

Finally, in Figure 5, we present plots for ethyne. At zero field, the ELF structure is similar to that reported elsewhere [2], with a characteristic ring structure about the triple bond. The ring is distorted at $0.1B_0$, splits into two at $0.5B_0$, and eventually becomes reminiscent of that for ethene at $1.0B_0$, with localisation above and below the bond.

The features of the cELF observed here can help to rationalise the success of the cTPSS meta-GGA functional in strong fields relative to conventional GGA functionals and also the local-density approximation (LDA), see Ref. [25]. In the cTPSS functional, the same modification of Eq. (12) is employed, entering the functional via $\alpha(\mathbf{r}) = [\tilde{\tau}_\sigma(\mathbf{r}) - \tau_\sigma^{\mathrm{vW}}(\mathbf{r})]/\tau_\sigma^{\mathrm{UEG}}(\mathbf{r})$ and $\tau_\sigma^{\mathrm{vW}}(\mathbf{r})/\tilde{\tau}_\sigma(\mathbf{r})$. Note that $\alpha(\mathbf{r})$ contains the same information as the cELF, to which it is related as $f_{\mathrm{ELF},\sigma}(\mathbf{r}) = 1/(1+\alpha_\sigma^2(\mathbf{r}))$. Hence $\alpha(\mathbf{r})$ also characterises the nature of different bonding regions, vanishing in one-orbital regions. However, it is not restricted to values between 0 and 1. The ratio $\tau_\sigma^{\mathrm{vW}}(\mathbf{r})/\tilde{\tau}_\sigma(\mathbf{r})$ also serves as a useful indicator of one-orbital regions.

Our visualisations suggest that, as the field increases, regions of large $f_{\mathrm{ELF}}(\mathbf{r})$ and low $\alpha(\mathbf{r})$ values distort considerably. Since meta-GGAs are designed to minimise one-electron self-interaction errors in these regions, the good performance of the cTPSS functional in strong magnetic fields observed in Ref. [25] may reflect an increased importance of these regions.

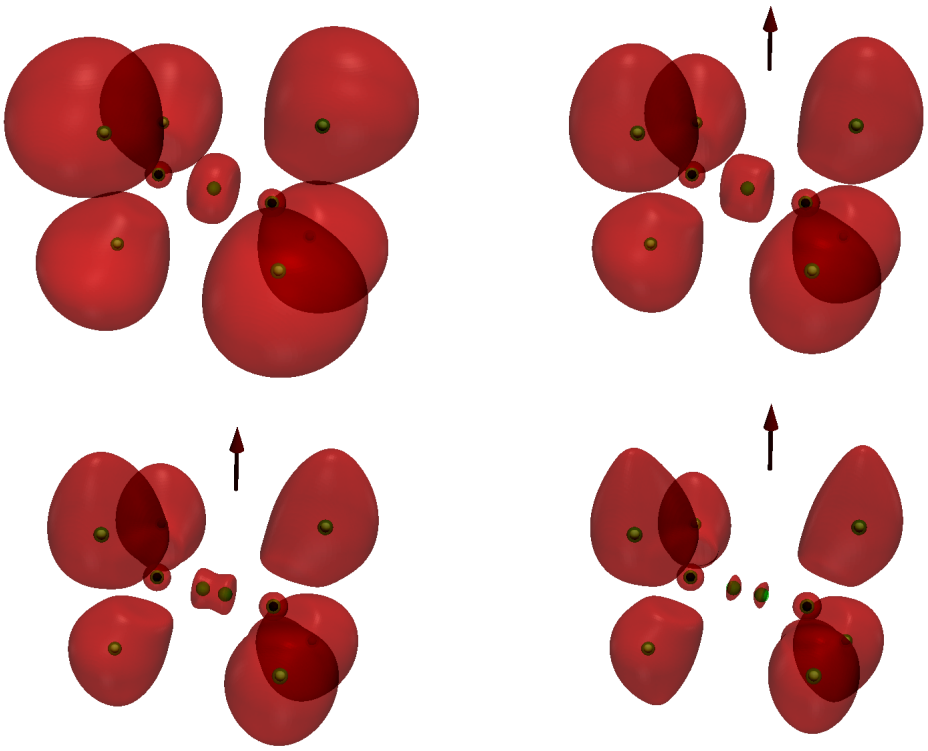

Figure 3. The cELF for ethane calculated at the cTPSS/u-aug-cc-pCVTZ at the corresponding zero-field geometry. The red iso-volumes depict the regions of $f_{\mathrm{ELF}} \geq 0.8$ for $0.0B_0$ (upper left), $0.4B_0$ (upper right), $0.7B_0$ (lower left), and $1.0B_0$ (lower right). Field direction is indicated by the red arrow.

3.2. *Topological Analysis*

The function f_{ELF} is a continuous scalar field and can therefore be subjected to a topological analysis similar to that used for the electron density by Bader [16]. This approach has been extensively used to highlight features of the ELF related to the chemical bonding in systems at zero field. In particular, the positions of attractors, which correspond to maxima of f_{ELF}, highlight regions of high localisation and are known to coincide with traditional chemical notions of bonding [2]. Changes in the number and arrangement of attractors in a magnetic field can therefore be indicative of deeper changes in the electronic structure induced by the field.

The attractors for ethane (determined on a uniform grid with spacing $0.05a_0$) are shown in Figure 3. At zero field and $0.4B_0$, a single attractor is present at the centre of the C-C bond. As the field increases, two attractors appear along the C-C bond axis, reflecting two separate maxima in the cELF. In Figure 4, the central dumb-bell shape of ethene encompasses two attractors. With increasing field strength, new features evolve, with two pairs of attractors appearing above and below the C=C bond.

In Figure 5, the attractors for ethyne are shown, the high symmetry of this system leading to a ring attractor about the bond. A magnetic field perpendicular to the bond axis destroys the linear symmetry, breaking the ring attractor into two point attractors. At $0.5B_0$, two further attractors appear above and below the C≡C bond axis. Finally, at $1.0B_0$, the cELF resembles that for ethene in the same field, with attractors above and below the C≡C bond axis.

3.3. *Physical Current Densities*

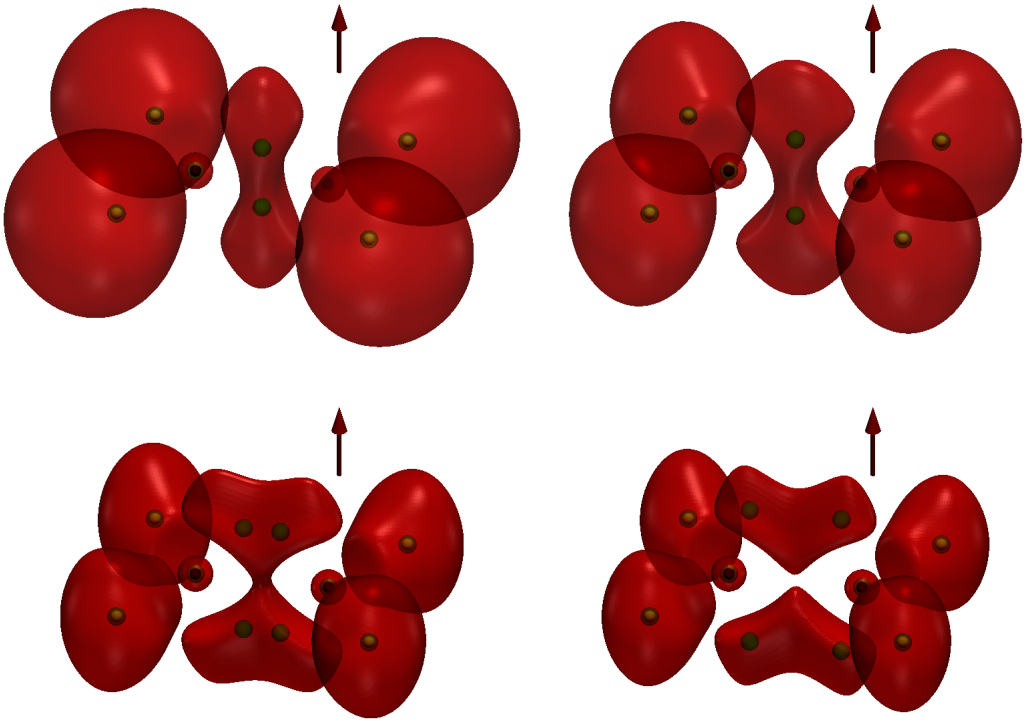

Figure 4. The cELF for ethene calculated at the cTPSS/u-aug-cc-pCVTZ at the corresponding zero-field geometry. The red iso-volumes depict the regions of $f_{\mathrm{ELF}} \geq 0.8$ for $0.0B_0$ (upper left), $0.4B_0$ (upper right), $0.7B_0$ (lower left), and $1.0B_0$ (lower right). Field direction is indicated by the red arrow.

The total physical current density $\mathbf{j}$ is the physically observable electron current induced by the magnetic field. It is related to the total paramagnetic current density that enters $\tilde{\tau} = \tilde{\tau}_\alpha + \tilde{\tau}_\beta$ (Eqs. (11) and (12)) and hence the cELF by

$$\mathbf{j}(\mathbf{r}) = \mathbf{j}_{\mathrm{p}}(\mathbf{r}) + \rho(\mathbf{r})\mathbf{A}(\mathbf{r}), \tag{15}$$

where the second term is the diamagnetic current, dependent on the magnetic vector potential related to the physical field $\mathbf{B}$ as $\mathbf{B} = \nabla \times \mathbf{A}$.

Visualisation of this quantity can aid with the understanding of the magnetic field's influence on a system. Figure 6 shows the physical current vector field superimposed over a cELF contour plot for ethyne at $1.0B_0$ in the molecular plane (left) and $1.15a_0$ above it (right). The current streamlines follow the structure of the cELF, circulating around the attractors and following contour regions of high localisation. In this sense, the current plots are complementary to the cELF, highlighting localised and bonding regions in a field. However, unlike the cELF, the current density vanishes in field-free DFT and is only of interest in a magnetic field.

4. Conclusions

We have presented the current-ELF (cELF), a generalisation of the ELF to systems in magnetic fields. The cELF constitutes a useful tool for understanding the nature of changes in chemical bonding upon application of a magnetic field. In systems bound by the perpendicular paramagnetic bonding mechanism [28], such as He_2, the effects of the field in confining the electronic structure in directions per-

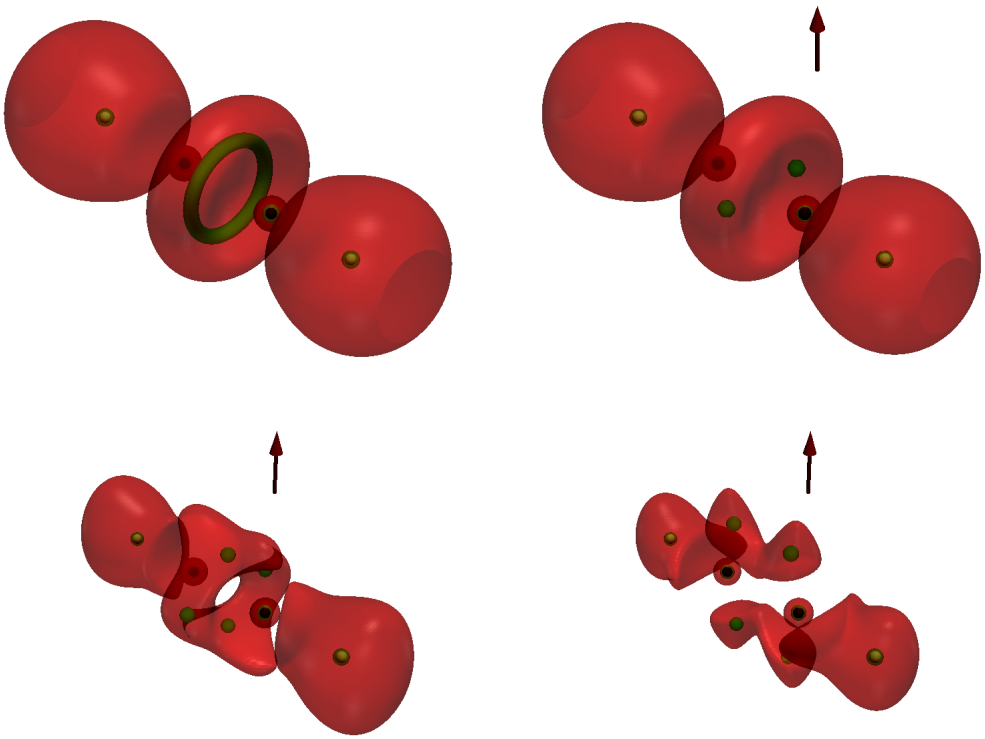

Figure 5. The cELF for ethyne calculated at the cTPSS/u-aug-cc-pCVTZ at the corresponding zero-field geometry. The red iso-volumes depict the regions of $f_{\mathrm{ELF}} \geq 0.8$ for $0.0B_0$ (upper left), $0.1B_0$ (upper right), $0.5B_0$ (lower left), and $1.0B_0$ (lower right). Field direction is indicated by the red arrow.

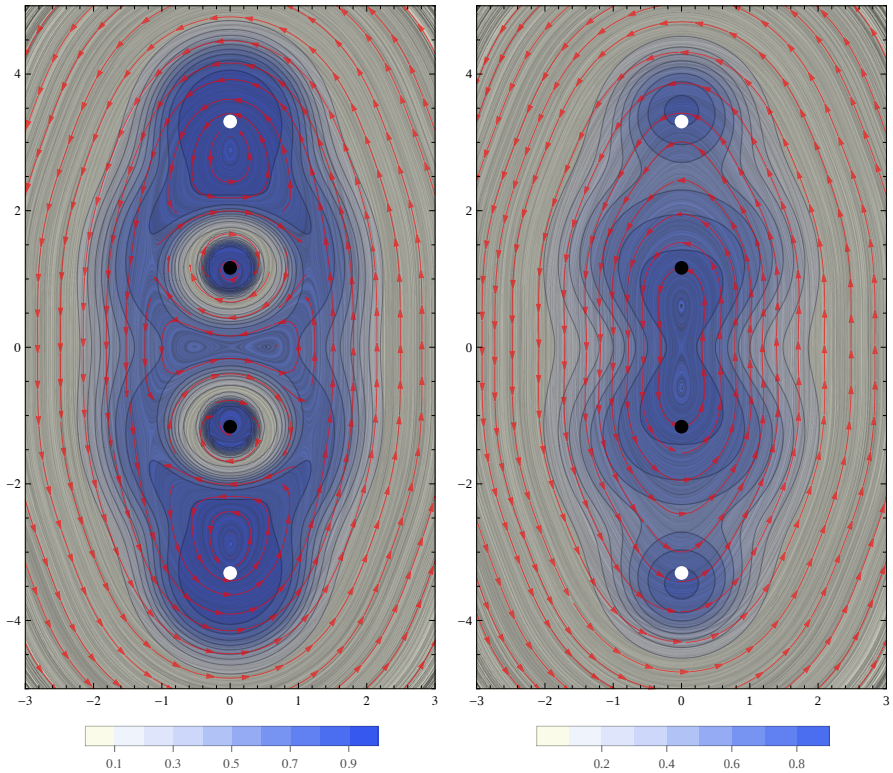

Figure 6. The physical current density (red stream lines) and the cELF (blue contours) of ethyne in the molecular plane (left) and $1.15a_0$ above it (right) in a perpendicular magnetic field of strength B_0.

pendicular to the field are particularly evident. For covalently bound systems, the effects are more subtle but the cELF provides a clear representation of field-induced changes in electronic structure, as illustrated by application to methane, ethane, ethene and ethyne. We expect cELF to become a useful tool for the interpretation of changes in chemical bonding and reactivity in magnetic fields.

Acknowledgements

It is a pleasure to dedicate this paper to Prof. Savin on the occasion of his 65th birthday. His infectious enthusiasm and willingness to openly share scientific thoughts and ideas continue to inspire further progress in the field. We look forward to many more inspiring collaborations in the future.

A. M. T. is grateful for support from the Royal Society University Research Fellowship scheme. We are grateful for access to the University of Nottingham High Performance Computing Facility. This work was supported by the Norwegian Research Council through the CoE Centre for Theoretical and Computational Chemistry (CTCC) Grant No. 179568/V30 and the Grant No. 171185/V30 and through the European Research Council under the European Union Seventh Framework Program through the Advanced Grant ABACUS, ERC Grant Agreement No. 267683.

References

[1] A. D. Becke and K. E. Edgecombe, *J. Chem. Phys.* **92**, 5397 (1990)
[2] B. Silvi and A. Savin, *Nature* **371**, 683 (1994)
[3] A. Savin and M. Kohout, *Int. J. Quantum Chem.* **60**, 875 (1996)
[4] A. Savin, A. D. Becke, J. Flad, R. Nesper, H. Preuss and H. G. von Schering, *Angew. Chem. Int. Ed. Engl.* **30**, 409 (1991)
[5] A. Savin, H. J. Flad, J. Flad, H. Preuss and H. G. von Schnering, *Angew. Chem. Int. Ed. Engl.* **31**, 185 (1992)
[6] H. Binder, I. Duttlinger, H. Loos, K. Locke, A. Pfitzner, H.-J. Flad, A. Savin and M. Kohout, *Zeitschrift fur Anorganische und Allgemeine Chemie* **621**, 400 (1995)
[7] X. Krokidis, V. Goncalves and A. Savin, *J. Phys. Chem. A* **102**, 5065 (1998)
[8] D. B. Chesnut, and A. Savin, *J. Am. Chem. Soc.* **121**, 2335 (1999)
[9] P. Fuentealba, and A. Savin, *J. Phys. Chem. A* **104**, 10882 (2000)
[10] A. Burkhardt, U. Wedig, H. G. von Schnering and A. Savin, *Zeitschrift fur Anorganische und Allgemeine Chemie* **619**, 437 (1993)
[11] R. Llusar, A. Beltran, J. Andres, B. Silvi and A. Savin, *J. Phys. Chem.* **99**, 12483 (1995)
[12] H. J. Flad, F. Schautz, Y. X. Wang, M. Dolg and A. Savin, *European Physical Journal D* **6**, 243 (1999)
[13] P. Fuentealba and A. Savin, *J. Phys. Chem. A* **105**, 11531 (2001)
[14] A. Savin, O. Jepsen, J. Flad, K. O. Andersen, H. Preuss and H. G. von Schnering, *Angew. Chem. Int. Ed. Engl.* **31**, 187 (1992)
[15] Y. Grin, U. Wedig, F. Wagner, H. G. von Schnering and A. Savin, *Journal of Alloys and Compounds* **255**, 203 (1997)
[16] R. F. W. Bader, S. Johnson, T.-H. Tang, P. L. A. Popelier, *J. Phys. Chem.*, **100**, 1539815415(1996)
[17] A. Savin, B. Silvi and F. Colonna, *Can. J. Chem* **74**, 1088 (1996)
[18] A. Savin, R. Nesper, S. Wengert and T. F. Fässler, *Angew. Chem. Int. Ed. Engl.* **36**, 1808 (1997)
[19] D. Marx, and A. Savin, *Angew. Chem. Int. Ed. Engl.* **36**, 2077 (1997)
[20] S. Noury, F. Colonna, A. Savin and B. Silvi, *J. Mol. Struct.* **450** 59 (1998)
[21] A. Savin, *J. Mol. Struct: THEOCHEM* **727**, 127 (2005)
[22] E. I. Tellgren, S. Kvaal, E. Sagvolden, U. Ekström, A. M. Teale and T. Helgaker, *Phys. Rev. A* **86**, 062506 (2012)

[23] E. I. Tellgren, A. M. Teale, J. W. Furness, K. K. Lange, U. Ekström and T. Helgaker, *J. Chem. Phys.* **140**, 034101 (2014)
[24] S. Reimann, U. Ekström, S. Stopkowicz, A. M. Teale, A. Borgoo, T. Helgaker, *Phys. Chem. Chem. Phys.* **17**, 18834 (2015)
[25] J. W. Furness, J. Verbeke, E. I. Tellgren, S. Stopkowicz, U. Ekström, T. Helgaker and A. M. Teale, *J. Chem. Theory Comput.* **11**, 4169 (2015)
[26] J. Tao, J. P. Perdew, V. Staroverov, G. E. Scuseria, *Phys. Rev. Lett.* **91**, 146401 (2003)
[27] J. E. Bates and F. Furche, *J. Chem. Phys.* **137**, 164105 (2012)
[28] K. K. Lange, E. I. Tellgren, M. R. Hoffmann, T. Helgaker, *Science* **80**, 327-331 (2012)
[29] A. D. Becke, *Int. J. Quantum Chem.* **23**, 19151922 (1983)
[30] J. F. Dobson, *J. Chem. Phys.* **94**, 4328 (1991)
[31] A. D. Becke, *J. Chem. Phys.* **117**, 6935 (2002)
[32] S. N. Maximoff and G. E. Scuseria, *Chem. Phys. Lett.* **390**, 408 (2004)
[33] J. Tao, *Phys. Rev. B* **71**, 205107 (2005)
[34] E. Sagvolden, U. Ekström, E. Tellgren, *Mol. Phys.*, **111**, 1295-1302 (2013)
[35] T. Burnus, M. A. L. Marques and E. K. U. Gross, *Phys. Rev. A* **71**, 010501(R) (2005)
[36] J. Pilm, E. Luppi, J. Bergs, C. Houe-Lvin and A. de la Lande, *J. Mol. Model.* **20**, 2368-2381(2014)
[37] F. J. London, *Phys. le Radium* **8**, 397-409 (1937)
[38] R. Ditchfield; *Mol. Phys.* **27** , 789807 (1974)
[39] R. Ditchfield; *Chem. Phys. Lett.* **65**, 31233133 (1976)
[40] LONDON, a quantum-chemistry program for plane-wave/GTO hybrid basis sets and finite magnetic field calculations. By E. Tellgren (primary author), T. Helgaker, A. Soncini, K. K. Lange, A. M. Teale, U. Ekstrm, S. Stopkowicz, and J. H. Austad. See londonprogram.org for more information.
[41] E. I. Tellgren, A. Soncini and T. Helgaker, *J. Chem. Phys.* **129**, 154114 (2008)
[42] U. Ekström, L. Visscher, R. Bast, A. J. Thorvaldsen, K. Ruud, *J. Chem. Theory Comput.* **6**, 1971 (2010)
[43] T. H. Dunning Jr., *J. Chem. Phys.* **90**, 1007 (1989)
[44] R. A. Kendall, T. H. Dunning Jr., R. J. Harrison, *J. Chem. Phys.* **96**, 6796 (1992)

The following image is the graphical abstract for the paper and offered for consideration as a cover image for the issue.

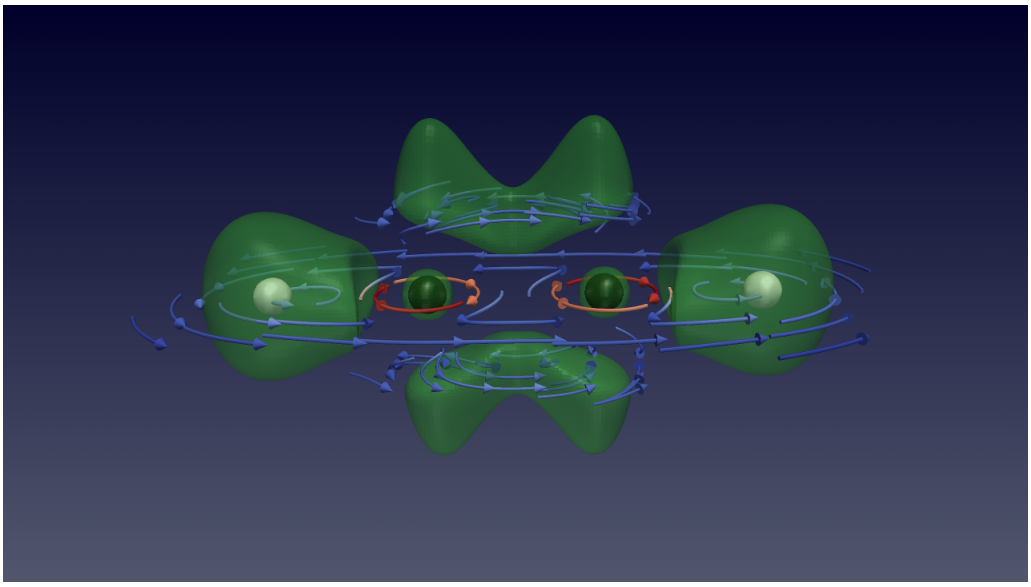

Figure 7. Graphical Abstract